

Comparative study on atomic and molecular Rydberg-state excitation in strong infrared laser fieldsHang Lv, Wanlong Zuo, Lei Zhao, Haifeng Xu,^{*} Mingxing Jin, and Dajun Ding[†]*Institute of Atomic and Molecular Physics, Jilin University, Changchun 130012, China**and Jilin Provincial Key Laboratory of Applied Atomic and Molecular Spectroscopy (Jilin University), Changchun 130012, China*Shilin Hu and Jing Chen[‡]*HEDPS, Center for Applied Physics and Technology, Collaborative Innovation Center of IFSA, Peking University, Beijing 100084, China**and Institute of Applied Physics and Computational Mathematics, P.O. Box 8009, Beijing 100088, China*

(Received 6 April 2015; revised manuscript received 20 February 2016; published 21 March 2016)

Rydberg-state excitation of atoms in strong infrared laser fields provides a new complementary aspect of the perspective of atom–strong field interactions. In this article, we perform an experimental and theoretical study on the corresponding process of diatomic molecules, N_2 and O_2 . We show that neutral molecules can also survive strong 800-nm laser fields in high Rydberg states, while their behavior is remarkably different in comparison with their companion atoms, Ar and Xe. The Rydberg excitation of N_2 generally behaves similarly to Ar, while that of O_2 is more significantly suppressed than the ionization compared to Xe in a high intensity region, which can be understood in the frame of a semiclassical picture, together with their different structures of molecular orbitals. However, distinct quantum features in the Rydberg excitation processes that are apparently beyond the semiclassical picture have been identified, i.e., the less suppressed probability of O_2 at low intensity and the oscillation behavior of the ratio between N_2 and Ar, indicating that our understanding of the relevant physics is still far from complete.

DOI: [10.1103/PhysRevA.93.033415](https://doi.org/10.1103/PhysRevA.93.033415)**I. INTRODUCTION**

When atoms and molecules are subjected to strong laser fields, they will undergo single or even multiple ionizations [1–3]. A semiclassical perspective has been established to understand various phenomena in atom–strong laser interactions, for example, above threshold ionization (ATI), nonsequential double ionization (NSDI), and high harmonic generation (HHG) [4,5]. Recently, it was surprising to find, both theoretically and experimentally, that neutral atoms in Rydberg states can survive strong laser fields [6,7], which has been the subject of elaborate experimental and theoretical studies in the past few years [8–16]. Besides atoms, Rydberg-state excitation (RSE) has also been observed in atomic fragments from the Coulomb explosion of dimers [17] and diatomic molecules [18].

In the semiclassical picture, the neutral atomic RSE is attributed to the capture of the tunneling electron into the Rydberg states under the interaction of a combined ionic Coulomb potential and laser fields, which is dubbed the recapture effect [6] or frustrated tunneling ionization (FTI) [7]. On the other hand, numerical calculations with the time-dependent Schrödinger equation (TDSE) [9,14] have shown that the probability of atomic RSE exhibits an oscillating function of the laser intensity, which cannot be explained by the semiclassical perspective. It is argued that the RSE can occur via Freeman resonance in which the electron is pumped to the Rydberg states via multiphoton absorption [9,14,19]. Unfortunately, to date, no quantum feature in the RSE in strong

laser fields has been observed, and the underlying mechanism of the process is still under debate.

A neutral RSE of molecules in strong laser fields has yet to be observed. Various studies have shown that the molecular structure plays an important role in strong-field single ionization [20–26], as well as the processes that are directly related to tunneling ionization, such as ATI [27–30] and NSDI [21,31–33]. A comparative study between a molecule and its companion atom [an atom with an ionization potential (IP) value that is similar to that of the molecule] will provide important information to reveal the underlying mechanism and to explore new features of a strong-field physical process. In this article, we show experimentally and theoretically that neutral diatomic molecules (N_2 and O_2) can survive strong 800-nm laser fields in Rydberg states. Compared to that of their companion atoms (Ar and Xe), remarkably different RSE probabilities of the molecules were observed. Analysis indicates that the semiclassical model, together with the structure of the molecular orbitals, can only partially explain the experimental observations, and some distinct quantum features beyond the semiclassical picture are clearly identified in the RSE process in strong laser fields.

II. EXPERIMENTAL SETUP

Because of their various decay processes, excited neutral molecules cannot be directly measured as the excited neutral atoms presented in Ref. [7], which have metastable states with lifetimes that are long enough to fly to the detector (typically hundreds of microseconds for a molecular beam). In our experiments, we applied a delayed static field ionization method to ionize the neutral Rydbergs, using a time-of-flight (TOF) mass spectrometer operated under a pulsed-electric-field mode. Experimentally, an effusive atomic or molecular beam through a leak valve was interacted by a focused

^{*}xuhf@jlu.edu.cn[†]dajund@jlu.edu.cn[‡]chen_jing@iapcm.ac.cn

Ti:sapphire femtosecond laser with a central wavelength of 800 nm and a pulse duration of 50 fs. After the directly ionized ions (M^+ , $M = \text{N}_2, \text{O}_2, \text{Ar}$, or Xe) were pushed away from the detector by an electric field, the remaining high-lying neutral Rydbergs (M^*) were field-ionized by another electric field with a delay time of typically 1.0 μs , and were detected by dual microchannel plates at the end of the flight, about 50 cm. In the case for detection of M^+ , standard dc electric fields were applied in the TOF mass spectrometer. The voltages in both cases were kept the same to ensure identical detection efficiencies for M^+ and $(M^*)^+$. This allows us to detect the neutral Rydberg states with $20 < n < 30$, estimated by a saddle-point model of static field ionization [$F = 1/(9n^4)$] [34]. The laser pulse energy was controlled by a half-wave plate and a Glan prism, before being focused into the vacuum chamber with a 250-mm lens. The peak intensity of the focused laser pulse was calibrated by comparing the measured saturation intensity of Xe with that calculated by the Ammosov-Delone-Krainov (ADK) model [35].

III. RESULTS AND DISCUSSION

In Figs. 1(a) and 1(b), we present the measured ion yields from Rydberg N_2^* vs Ar^* and O_2^* vs Xe^* , respectively, using a linearly polarized 800-nm light. For comparison, data of the corresponding singly charged ions are also shown in each panel, which well reproduce the previous experimental measurements [20,21,25]. The results clearly show that, similar to strong-field single ionization, it exhibits a significant suppression of Rydberg formation in O_2 compared to Xe , while N_2 and Ar have comparable probabilities at all the laser intensities used in the experiment.

In order to compare more clearly the RSE behaviors of molecules with the ionization process, we plot the ratios of Rydberg and ionization yields, N_2^*/Ar^* and N_2^+/Ar^+ in Fig. 1(c) and O_2^*/Xe^* and O_2^+/Xe^+ in Fig. 1(d), respectively. The ratios of both N_2^*/Ar^* and N_2^+/Ar^+ are around 1, irrespective of the laser intensity, however, N_2^*/Ar^* shows a distinct bump structure compared with the smooth curve of N_2^+/Ar^+ . For O_2 and Xe , both ratios of O_2^*/Xe^* and O_2^+/Xe^+

show suppression and, more interestingly, the ratio of O_2^*/Xe^* is apparently smaller than that of O_2^+/Xe^+ in the whole laser intensity region considered, showing that the suppression in the RSE is stronger than that in the ionization.

To compare with the observed data, we numerically solve TDSE with B splines and the Crank-Nicolson method [36,37], and the single-active-electron model potentials [38,39] (the details of the calculation method can be found in the appendix). After the end of the pulse, we calculate the Rydberg-state population and ionization probability by projecting the wave function onto the corresponding field-free eigenstates. To simplify the calculation, the molecular axis is assumed to be parallel to the polarization direction of the laser field (parallel alignment).

The calculated results are shown in Fig. 2. Both the single ionization and RSE of N_2 and Ar well reproduce the experimental results [see Figs. 1(a) and 1(c)]. The ratio N_2^+/Ar^+ shows a smooth curve, but N_2^*/Ar^* oscillates around 1, corresponding to the observed bump structure in Fig. 1(c), which may be a portion of an oscillation curve of which the low intensity region is beyond the detection limit in the current experiment. For O_2 and Xe , the calculation reproduces the observed stronger suppression of O_2^*/Xe^* with respect to O_2^+/Xe^+ at the high intensity region. At the low intensity region, on the other hand, the calculation shows that O_2^*/Xe^* will exceed O_2^+/Xe^+ , indicating that the RSE will become less suppressed compared with the ionization process.

As mentioned above, there are two possible mechanisms for the RSE process, i.e., the Freeman resonance [9,19], and the recapture effect [6] or FTI [7]. The dependence of the excited neutral atom on ellipticity and the consistency between the TDSE and semiclassical simulation on populations of Rydberg states tend to support the FTI mechanism [7,40]. It is noteworthy that, if resonance were the underlying mechanism, the suppression for O_2 should be unexpected since

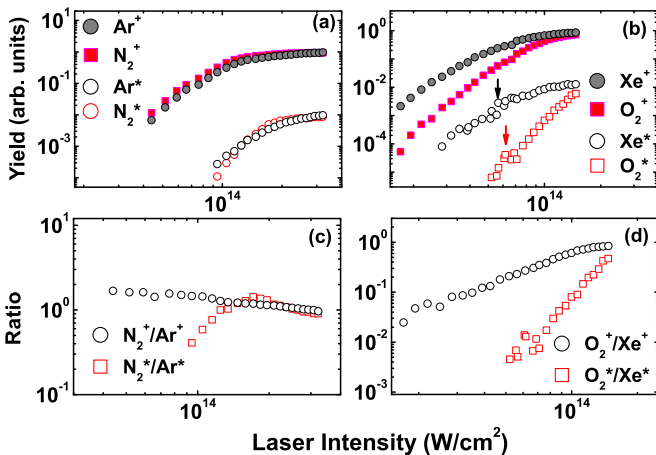


FIG. 1. (a) and (b) Experimentally measured single ionization and Rydberg excitation yields (see text). (c) and (d) Ratios of single ionization and Rydberg excitation yields.

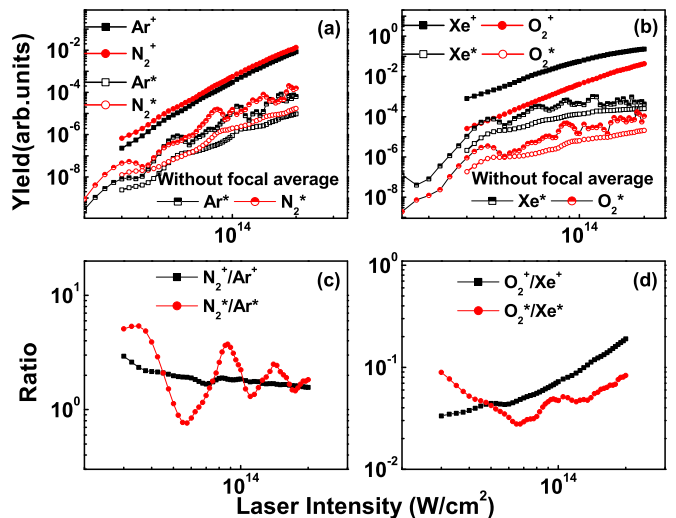


FIG. 2. (a) and (b) Calculated single ionization and Rydberg excitation yields with focal average. The Rydberg excitation without focal average is also shown (see text). (c) and (d) Ratios of single ionization and Rydberg excitation yields.

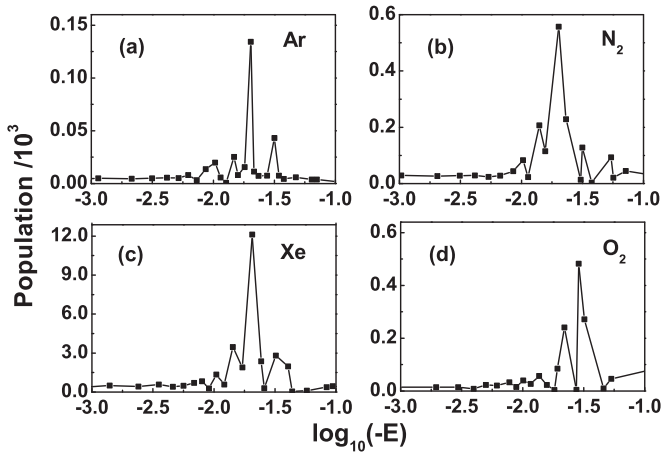


FIG. 3. Calculated distributions of populated Rydberg states after the laser pulse is over. For Ar and N₂, laser intensity $I = 1.2 \times 10^{14}$ W/cm². For Xe and O₂, $I = 1 \times 10^{14}$ W/cm².

Ar, N₂, Xe, and O₂ possess similar Rydberg levels owing to the large orbits of the almost decoupled electron, noting that the Freeman resonance structures have been identified experimentally for both molecules [41,42]. Therefore, the simultaneous appearance or absence of the suppression of the RSE, compared with ionization for accompanied atoms and molecules, indicates that the Rydberg states populated after an interaction with the infrared intense laser field come from the photoelectron that first tunnels out through the barrier formed by the Coulomb potential and the external laser field, and then is trapped by the Coulomb potential in the way it goes out.

To further understand the difference between atomic and molecular RSE, we plot populations of Rydberg states of different species after the laser pulse is over in Fig. 3. All distributions show a peak structure, however, the positions of the peaks for N₂, Ar, and Xe locate at about energy of -0.02 a.u. while the peak of O₂ is at -0.029 a.u. This observation indicates that, compared with other species, the electron tends to occupy lower Rydberg states in O₂. In Fig. 4, we show the spatial distributions of the populated

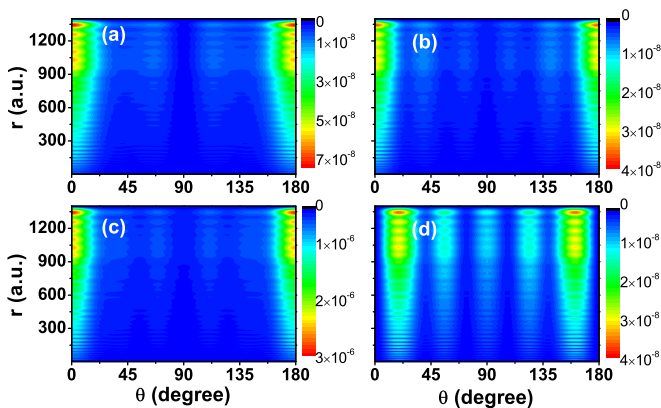


FIG. 4. Spatial distribution of Rydberg states in the region of -0.001 a.u. $< E < 0$. (a) Ar, (b) N₂, (c) Xe, and (d) O₂. Laser intensity $I = 1 \times 10^{14}$ W/cm².

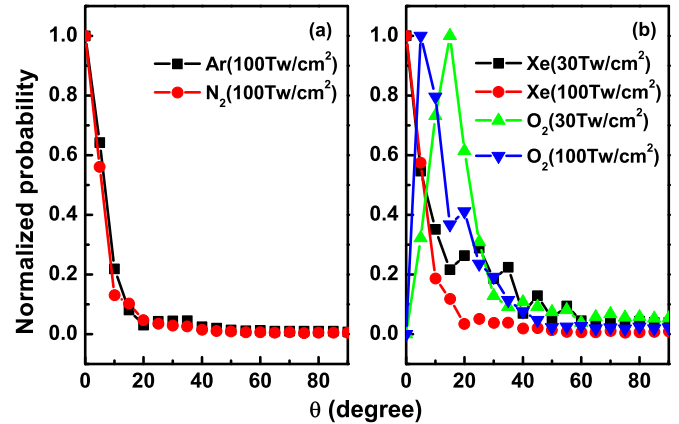


FIG. 5. Calculated angular distributions of photoelectrons with respect to the polarization direction of the laser field (0°).

Rydberg state from an energy of -0.001 a.u. to 0 . Again, the distributions of N₂, Ar, and Xe look very similar, but the one of O₂ shows a pronounced difference. The distributions of atoms and N₂ have maxima in the field direction (0° and 180°), while for O₂ the maximum shifts to about 20° . This apparent deviation from the laser field direction of the spatial distribution of O₂* indicates a further intrinsic difference between the behaviors of O₂ and other species in the RSE process.

In Fig. 5, we further show angular distributions of photoelectrons ejected in the single ionization for all species, which are obtained by the flux analysis approach [43]. The photoelectrons highly concentrate in the field direction [with a full width at half maximum (FWHM) of about 10°] for N₂, Ar, and Xe. In contrast, the maximum of the angular distribution of O₂ locates at about 15° at an intensity of 3×10^{13} W/cm² and shifts to about 6° when the intensity increases to 1×10^{14} W/cm². This difference between the angular distributions of N₂ and O₂ is attributed to their different highest occupied molecular orbitals (HOMOs) ($3\sigma_g$ for N₂ and $1\pi_g$ for O₂, respectively) [31,44]. Apparently, there is a good correspondence between the photoelectron angular distribution and the spatial angular distribution of the populated Rydberg states. According to the above analysis, the Rydberg states are populated by electrons during their ejection process after tunneling out of the barrier. So, for atoms and N₂, the electrons will populate the Rydberg states with maxima in the field direction since the electrons go out mainly in the field direction. For O₂, since the peak of the angular distribution of electrons deviates from the field direction, they will tend to occupy the Rydberg states with a maximum at other angles [45].

Moreover, the FWHM of the angular distribution of O₂ ($\sim 20^\circ$) is noticeably wider than those of other species. This explains the more pronounced suppression of the RSE compared with the ionization for O₂. Compared with other species, a wider angular distribution leads to a stronger diffusion of the wave packet of the electron ionized from O₂ when it evolves in the laser field. Therefore, it will be harder for the electron to occupy high Rydberg states which locate relatively farther from the ionic core, leading to peaks of

the energy distributions of populated Rydberg states at lower-energy levels and a relatively smaller population of Rydberg states in the energy region of $-0.001 \text{ a.u.} < E < 0$, which is far away from the ionic core (see Fig. 4). It should be mentioned here that this particular photoelectron angular distribution has also been shown to be responsible for the suppression of the NSDI ratio and the relatively wider differential angular distribution at a cutoff energy in the high-order ATI of O_2 compared with atoms and the N_2 molecule [29,31].

Despite the fact that only parallel alignment is considered in our calculation, the main result will not be affected by this limitation. For N_2 , the angular distribution always peaks at the field direction, irrespective of the alignment angle, which is very similar to atoms [44]. So, according to our analysis, the RSE will also be similar to Ar even when the other alignment angles are taken into account despite the decreasing ionization rate with increasing alignment angle [46]. For O_2 , the electron is always ejected off the field direction, except at some specific alignment angles. Moreover, the angular distribution of O_2 is usually wider than that of N_2 and atoms [44]. Therefore, the above analysis of the mechanism for the RSE suppression of O_2 compared with Xe is expected to be valid when other alignment angles are considered.

Nevertheless, the above mechanism cannot explain the less suppression of O_2^* with respect to Xe^* compared with the ionization at low intensity [Fig. 2(d)]. As shown in Fig. 5(b), the angular distribution of the photoelectron from O_2 is even wider at low intensity than that at high intensity, which should result in more suppression, according to the semiclassical perspective, which is in contradiction with the theoretical results in Fig. 2(d). It should be noted that, in this low intensity regime, i.e., the multiphoton regime [the Keldysh parameter $\gamma = (I_p/2U_p)^{1/2} > 1$], the FTI picture may become invalid and the Freeman resonance mechanism plays an increasingly important role, leading to the disappearance of the RSE suppression. Another distinct quantum characteristic that cannot be explained by the semiclassical picture is the oscillation behavior of the ratio N_2^*/Ar^* shown in Figs. 1(c) and 2(c). The origin of the oscillation can be more clearly understood by looking at the yields of Ar^* and N_2^* without a focal average, depicted also in Fig. 2(a). Both curves show apparent peak structures consisting of high and low peaks which appear alternatively. In addition, though the peaks in both curves almost coincide with each other, the high and low peaks appear in a reverse sequence in two curves, resulting in the oscillations in the ratio of two curves. In contrast, for Xe^* and O_2^* , though both curves also show an oscillating structure, the sequences of high and low peaks appear simultaneously, as depicted in Fig. 2(b), and the TDSE results without focal average. Thus, the oscillation behavior is absent for the ratio of O_2^*/Xe^* . It is interesting to note that the intervals between these peaks are all about $2.5 \times 10^{13} \text{ W/cm}^2$, which corresponds to a ponderomotive energy $U_p = 1.5 \text{ eV} \simeq \hbar\omega$, the photon energy of the laser field. This feature, which can be also found in the quantum calculation of Ref. [9], indicates some processes related to the Freeman resonance in the Rydberg excitation. It is worthwhile mentioning that these peaks cannot be distinguished in the experiments and calculations after the focal average, however, hump structures, which are the residues of these peaks after

focal average, can still be seen in the calculation results [see Figs. 2(a) and 2(b)] and the experimental data of Xe and O_2 [denoted by arrows in Fig. 1(b)], and the apparent oscillations appearing in both Figs. 1(c) and 2(c). Moreover, this quantum feature also implies a relationship between the RSE and another phenomenon named ‘‘resonancelike enhancement (RLE)’’ in high-order ATI, which is believed to be a pure quantum-mechanical effect, and its underlying mechanism is still under debate [47–50]. In the RLE process, it is also found that N_2 behaves similarly to Ar while O_2 shows pronounced suppression compared with Xe [30]. The similarity between the RSE and RLE processes indicates that another important quantum effect, i.e., the interference effect, which has been identified to be essential in the molecular ionization process [23,25,30], may also play an important role in the molecular RSE process.

IV. CONCLUSIONS

In conclusion, we have shown that, similar to atoms, neutral diatomic molecules can also survive strong 800-nm laser fields in high Rydberg states. We have observed the suppressed RSE probability in O_2 compared to Xe, and the suppression is stronger than the ionization process. For the RSE of N_2 , though it generally behaves similar to Ar, the ratio N_2^*/Ar^* shows oscillation behavior compared with the ionization probability. The TDSE calculations well reproduce the experimental measurements of N_2 and Ar. For O_2 and Xe, the theoretical result that qualitatively reproduces the more strongly suppressed RSE compared to the ionization at high intensity, however, predicts that the RSE becomes less suppressed at low intensity. Analysis indicates that the experimental observations can be partially explained by the FTI mechanism, together with the structure of molecular orbitals; however, distinct quantum features, which are beyond the semiclassical picture, manifest in the RSE process and demand further investigation in the future.

ACKNOWLEDGMENTS

The authors acknowledge X. Liu for helpful discussions. This work was supported by the National Basic Research Program of China (No. 2013CB922200) and NNSFC (No. 11534004, No. 11034003, No. 11274140, No. 11274050, No. 11334009, and No. 11425414).

APPENDIX: NUMERICAL METHODS

In this appendix, we give the details of the theoretical method adopted in our article. Within a single-active-electron approximation, the TDSE equation in the length gauge for atoms and molecules is given by

$$i \frac{\partial}{\partial t} \Psi(\mathbf{r}, t) = \left\{ -\frac{1}{2r^2} \frac{\partial}{\partial r} r^2 \frac{\partial}{\partial r} + \frac{1}{2r^2} \left[\frac{\partial}{\partial \xi} (1 - \xi^2) \frac{\partial}{\partial \xi} - \frac{m^2}{1 - \xi^2} \right] + V(r) - \mathbf{r} \cdot \mathbf{E}(t) \right\} \Psi(\mathbf{r}, t), \quad (\text{A1})$$

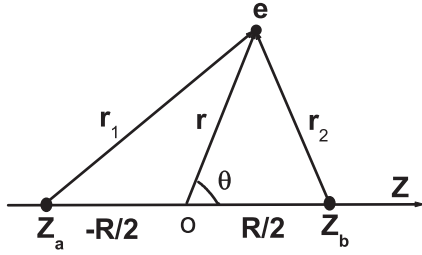


FIG. 6. Coordinates of the diatomic molecule.

where $\xi = \cos \theta$, and m is the z component of the electronic orbital momentum. For atoms, the effective model potential is written as

$$V(r) = -(1 + a_1 e^{-a_2 r} + a_3 r e^{-a_4 r} + a_5 e^{-a_6 r})/r. \quad (\text{A2})$$

For the Ar atom, $a_1 = 16.039$, $a_2 = 2.007$, $a_3 = -25.543$, $a_4 = 4.525$, $a_5 = 0.961$, and $a_6 = 0.443$ [38]. For the Xe atom, $a_1 = 51.356$, $a_2 = 2.112$, $a_3 = -99.927$, $a_4 = 3.737$, $a_5 = 1.644$, and $a_6 = 0.431$ [38].

For the diatomic molecule N_2 (see Fig. 6), the potential is [51]

$$V(r) = \sum_{\alpha=1}^2 \left\{ -\frac{0.5}{|\vec{r}_\alpha|} - \frac{29.5}{h[\exp(|\vec{r}_\alpha|/d) - 1]|\vec{r}_\alpha| + |\vec{r}_\alpha|} \right\}, \quad (\text{A3})$$

where $\vec{r}_\alpha = \vec{r} \pm \frac{\vec{R}}{2}$, and the parameters h and d are 24.25 and 1.311, respectively.

For O_2 (see Fig. 6), the used form of the model potential is [39]

$$V(r) = \sum_{\alpha=1}^2 \frac{-Z_\alpha(\vec{r}_\alpha)}{\sqrt{|\vec{r}_\alpha|^2 + a_\alpha}}, \quad (\text{A4})$$

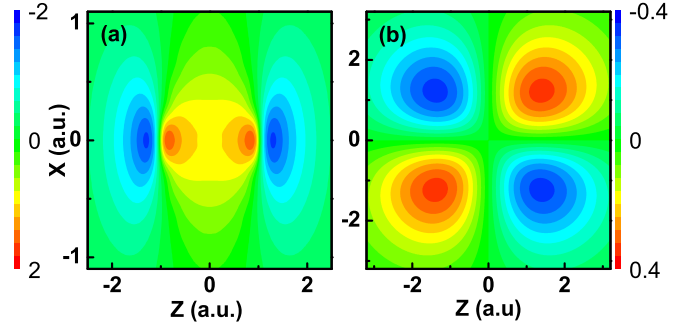
where the analytical form of $Z_\alpha(\vec{r}_\alpha)$ is

$$Z_\alpha(\vec{r}_\alpha) = 0.5 + (Z_\alpha^0 - 0.5) \exp\left[-\frac{|\vec{r}_\alpha|^2}{\sigma_\alpha^2}\right], \quad (\text{A5})$$

with $a_\alpha = 20$, $Z_\alpha^0 = 8$, and $\sigma_\alpha = 2.54$. The wave functions in the present work are expanded in terms of the B splines as follows [36]:

$$\Psi(t, r, \xi, \phi) = \frac{1}{\sqrt{2\pi}} \sum_{\mu\nu} C_{\mu\nu}(t) \frac{B_\mu^k(r)}{r} (1 - \xi^2)^{\frac{|m|}{2}} B_\nu^k(\xi) e^{im\phi}. \quad (\text{A6})$$

$B_\mu^k(r)$ is the B spline of order $k = 7$ [37]. The direction of laser polarization is parallel to the molecular axis, and the vector potential is $A(t) = \frac{E_0}{\omega} \sin^2(\frac{\pi t}{T}) \cos(\omega t)$, $0 < t < T$. E_0 is the peak laser field, and T and ω are the duration and the frequency of the laser pulse, respectively. The time-dependent electric field is defined as $E(t) = -\frac{\partial A(t)}{\partial t}$. The time-dependent wave functions are propagated by the Crank-Nicolson method

FIG. 7. Two-dimensional distribution of the wave function for the initial state: (a) N_2 , (b) O_2 .

[36,37] and the photoelectron angular distribution is obtained by flux analysis [43],

$$\frac{dP}{d\Omega} = \int_T^{T+t_0} dt r_0^2 j_r(r_0, \Omega, t), \quad (\text{A7})$$

where the radial probability current $j_r(r_0, \Omega, t)$ of the time-dependent wave function is written in terms of the B splines as

$$j_r(r, \xi, \phi, t) = \frac{1}{2\pi} \frac{1}{r^2} \text{Im} \sum_{\mu_1 \nu_1} \sum_{\mu_2 \nu_2} C_{\mu_1 \nu_1}^*(t) C_{\mu_2 \nu_2}(t) B_{\mu_1}^k(r) \times \frac{\partial B_{\mu_2}^k(r)}{\partial r} (1 - \xi^2)^{(|m_1| + |m_2|)/2} B_{\nu_1}^k(\xi) \times B_{\nu_2}^k(\xi) e^{i(m_2 - m_1)\phi}. \quad (\text{A8})$$

Since the laser field is parallel to the molecular axis in our calculation, the magnetic quantum number m is preserved and m_1 is equal to m_2 in Eq. (A7). In our calculations, 1200 radial B splines and 20 angular B splines are adopted and the truncated radial r_{max} is 1400 a.u. The central frequency of the laser field is $\omega = 0.057$ a.u. and the pulse duration is 10 cycles. The time step is $\delta t = 0.08$ a.u. in our calculation. The probability current is calculated at a distance $r_0 = 600$ a.u. and is integrated over time up to $t_0 = 500$ a.u. after the end of the laser pulse. Convergence is achieved with the above settings.

Initial states of atoms and molecules

For Ar and Xe, the ionization potentials of the initial $3p$ and $5p$ states obtained in our calculation are 15.75 and 12.04 eV, respectively, which agree well with the real ionization potentials of the $3p$ (15.76 eV) state of Ar and the $5p$ (12.13 eV) state of Xe [52]. For N_2 , assuming the internuclear distance to be the equilibrium value $R = 2.08$ a.u., the calculated ionization potential of the initial $3\sigma_g$ orbital is 15.56 eV. For O_2 , the internuclear distance is $R = 2.28$ a.u. (equilibrium value) and the calculated ionization potential of the initial $1\pi_g$ orbital is 12.05 eV. Both are in good accordance with the real ionization potentials of the $3\sigma_g$ orbital (15.58 eV) of N_2 and the $1\pi_g$ orbital (12.07 eV) of O_2 [52]. The wave functions of the two molecules are plotted in Fig. 7.

[1] P. Agostini, F. Fabre, G. Mainfray, G. Petite, and N. K. Rahman, *Phys. Rev. Lett.* **42**, 1127 (1979).

[2] W. Becker, F. Grasbon, R. Kopold, D. B. Milošević, G. G. Paulus, and H. Walther, *Adv. At. Mol. Opt. Phys.* **48**, 35 (2002).

- [3] W. Becker, X. Liu, P. Ho, and J. H. Eberly, *Rev. Mod. Phys.* **84**, 1011 (2012).
- [4] K. J. Schafer, B. Yang, L. F. DiMauro, and K. C. Kulander, *Phys. Rev. Lett.* **70**, 1599 (1993).
- [5] P. B. Corkum, *Phys. Rev. Lett.* **71**, 1994 (1993).
- [6] B. B. Wang, X. F. Li, P. M. Fu, J. Chen, and J. Liu, *Chin. Phys. Lett.* **23**, 2729 (2006).
- [7] T. Nubbemeyer, K. Gorling, A. Saenz, U. Eichmann, and W. Sandner, *Phys. Rev. Lett.* **101**, 233001 (2008).
- [8] U. Eichmann, T. Nubbemeyer, H. Rottke, and W. Sandner, *Nature (London)* **461**, 1261 (2009).
- [9] E. A. Volkova, A. M. Popov, and O. V. Tikhonova, *Sov. Phys. JETP* **113**, 394 (2011).
- [10] A. Emmanouilidou, C. Lazarou, A. Staudte, and U. Eichmann, *Phys. Rev. A* **85**, 011402(R) (2012).
- [11] A. von Veltheim, B. Manschwetus, W. Quan, B. Borchers, G. Steinmeyer, H. Rottke, and W. Sandner, *Phys. Rev. Lett.* **110**, 023001 (2013).
- [12] K. Y. Huang, Q. Z. Xia, and L. B. Fu, *Phys. Rev. A* **87**, 033415 (2013).
- [13] S. Eilzer, H. Zimmermann, and U. Eichmann, *Phys. Rev. Lett.* **112**, 113001 (2014).
- [14] Q. G. Li, X. M. Tong, T. Morishita, H. Wei, and C. D. Lin, *Phys. Rev. A* **89**, 023421 (2014).
- [15] U. Eichmann, A. Saenz, S. Eilzer, T. Nubbemeyer, and W. Sandner, *Phys. Rev. Lett.* **110**, 203002 (2013).
- [16] H. Zimmermann, J. Buller, S. Eilzer, and U. Eichmann, *Phys. Rev. Lett.* **114**, 123003 (2015).
- [17] J. Wu, A. Vredenburg, B. Ulrich, L. P. H. Schmidt, M. Meckel, S. Voss, H. Sann, H. Kim, T. Jahnke, and R. Dörner, *Phys. Rev. Lett.* **107**, 043003 (2011).
- [18] B. Manschwetus, T. Nubbemeyer, K. Gorling, G. Steinmeyer, U. Eichmann, H. Rottke, and W. Sandner, *Phys. Rev. Lett.* **102**, 113002 (2009).
- [19] R. R. Freeman, P. H. Bucksbaum, H. Milchberg, S. Darack, D. Schumacher, and M. E. Geusic, *Phys. Rev. Lett.* **59**, 1092 (1987).
- [20] A. Talebpour, C.-Y. Chien, and S. L. Chin, *J. Phys. B* **29**, L677 (1996).
- [21] C. Guo, M. Li, J. P. Nibarger, and G. N. Gibson, *Phys. Rev. A* **58**, R4271(R) (1998).
- [22] C. Guo, *Phys. Rev. Lett.* **85**, 2276 (2000).
- [23] J. Muth-Böhm, A. Becker, and F. H. M. Faisal, *Phys. Rev. Lett.* **85**, 2280 (2000).
- [24] X. M. Tong, Z. X. Zhao, and C. D. Lin, *Phys. Rev. A* **66**, 033402 (2002).
- [25] Z. Y. Lin, X. Y. Jia, C. L. Wang, Z. L. Hu, H. P. Kang, W. Quan, X. Y. Lai, X. J. Liu, J. Chen, B. Zeng, W. Chu, J. P. Yao, Y. Cheng, and Z. Z. Xu, *Phys. Rev. Lett.* **108**, 223001 (2012).
- [26] H. P. Kang, Z. Y. Lin, S. P. Xu, C. L. Wang, W. Quan, X. Y. Lai, X. J. Liu, X. Y. Jia, X. L. Hao, J. Chen, W. Chu, J. P. Yao, B. Zeng, Y. Cheng, and Z. Z. Xu, *Phys. Rev. A* **90**, 063426 (2014).
- [27] F. Grasbon, G. G. Paulus, S. L. Chin, H. Walther, J. Muth-Bohm, A. Becker, and F. H. M. Faisal, *Phys. Rev. A* **63**, 041402(R) (2001).
- [28] M. Okunishi, R. Itaya, K. Shimada, G. Prumper, K. Ueda, M. Busuladzic, A. Gazibegovic-Busuladzic, D. B. Milosevic, and W. Becker, *Phys. Rev. Lett.* **103**, 043001 (2009).
- [29] H. Kang, W. Quan, Y. Wang, Z. Lin, M. Wu, H. Liu, X. Liu, B. B. Wang, H. J. Liu, Y. Q. Gu, X. Y. Jia, J. Liu, J. Chen, and Y. Cheng, *Phys. Rev. Lett.* **104**, 203001 (2010).
- [30] W. Quan, X. Y. Lai, Y. J. Chen, C. L. Wang, Z. L. Hu, X. J. Liu, X. L. Hao, J. Chen, E. Hasovic, M. Busuladzic, W. Becker, and D. B. Milosevic, *Phys. Rev. A* **88**, 021401(R) (2013).
- [31] X. Y. Jia, W. D. Li, J. Y. Fan, J. Liu, and J. Chen, *Phys. Rev. A* **77**, 063407 (2008); X. Y. Jia, D. H. Fan, W. D. Li, and J. Chen, *Chin. Phys. B* **22**, 013303 (2013).
- [32] D. Zeidler, A. Staudte, A. B. Bardon, D. M. Villeneuve, R. Dörner, and P. B. Corkum, *Phys. Rev. Lett.* **95**, 203003 (2005).
- [33] Y. Li, S. P. Yang, J. Fan, and J. Chen, *J. Phys. B* **47**, 045601 (2014).
- [34] Though just a portion of the neutral Rydbergs can be ionized and detected, our theoretical results indicate that the main results in this article remain unchanged for different n -Rydbergs.
- [35] M. V. Ammosov, N. B. Delone, and V. P. Krainov, *Sov. Phys. JETP* **64**, 1191 (1986).
- [36] S. L. Hu, Z. X. Zhao, and T. Y. Shi, *Int. J. Quantum Chem.* **114**, 441 (2014).
- [37] H. Bachau, E. Cormier, P. Decleva, J. E. Hansen, and F. Martin, *Rep. Prog. Phys.* **64**, 1815 (2001).
- [38] D. B. Milošević, W. Becker, M. Okunishi, G. Prümper, K. Shimada, and K. Ueda, *J. Phys. B* **43**, 015401 (2010).
- [39] M. Peters, T. T. Nguyen-Dang, E. Charron, A. Keller, and O. Atabek, *Phys. Rev. A* **85**, 053417 (2012).
- [40] The ellipticity dependence of Rydberg excitation of four species is also measured in our experiment. The results are similar to those of Ref. [7] and will be presented elsewhere.
- [41] G. N. Gibson, R. R. Freeman, and T. J. McIlrath, *Phys. Rev. Lett.* **67**, 1230 (1991).
- [42] T. Kłoda, A. Matsuda, H. O. Karlsson, M. Elshakre, P. Linusson, J. H. D. Eland, R. Feifel, and T. Hansson, *Phys. Rev. A* **82**, 033431 (2010).
- [43] L. B. Madsen, L. A. A. Nikolopoulos, T. K. Kjeldsen, and J. Fernández, *Phys. Rev. A* **76**, 063407 (2007).
- [44] D. B. Milošević, *Phys. Rev. A* **74**, 063404 (2006).
- [45] This picture can also be understood by considering the angular momentum conservation in the process. In the linear polarized laser field, the magnetic quantum number (m) is conserved in the process. For atoms and N_2 , the largest contribution comes from the outmost orbitals (e. g., $3\sigma_g$ for the HOMO orbital of N_2) with $m = 0$. So, the final populated Rydberg states also possess $m = 0$, which have maxima in the field direction. For O_2 , $m = 1$ for the HOMO orbital ($1\pi_g$), so only Rydberg states with $m = 1$, which have maxima at other directions, can be occupied.
- [46] D. Pavičić, K. F. Lee, D. M. Rayner, P. B. Corkum, and D. M. Villeneuve, *Phys. Rev. Lett.* **98**, 243001 (2007).
- [47] H. G. Muller and F. C. Kooiman, *Phys. Rev. Lett.* **81**, 1207 (1998); H. G. Muller, *ibid.* **83**, 3158 (1999); *Phys. Rev. A* **60**, 1341 (1999).
- [48] R. Kopold and W. Becker, *J. Phys. B* **32**, L419 (1999).
- [49] J. Wassaf, V. Vénard, R. Taïeb, and A. Maquet, *Phys. Rev. Lett.* **90**, 013003 (2003).
- [50] C. C. Wang *et al.*, *Phys. Rev. A* **90**, 023405 (2014).
- [51] K. J. Miller and A. E. S. Green, *J. Chem. Phys.* **60**, 2617 (1974).
- [52] [<http://www.nist.gov/index.html>].